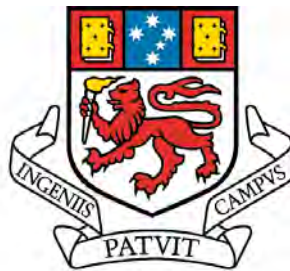


**Genesis of the Rosebery massive sulphide deposit,
western Tasmania, Australia.**

by

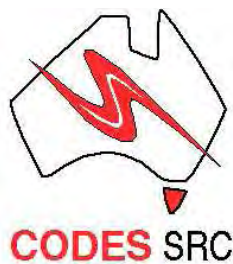
Neil K. Martin (BSc. Hons.)

**Submitted in fulfilment of the requirements for the
degree of Doctor of Philosophy**



UNIVERSITY OF TASMANIA

September, 2004



Declaration

This thesis contains no material that has been accepted for a degree or diploma by the University or any other institution, except by way of background information and duly acknowledged in the thesis, and to the best of the candidate's knowledge and belief, contains no material previously published or written by another person, except where due acknowledgement is made in the text of the thesis.

Neil K. Martin

Date:

Confidentiality

This thesis is not to be made available for loan or copying for two years following the date this statement was signed. Following that time, the thesis may be made available for loan and limited copying in accordance with the *Copyright Act 1969*.

Neil K. Martin

Date:

Abstract

The Rosebery massive sulphide deposit, with historical production and current resources of ~32.7Mt @ at 14.5% Zn, 4.4% Pb, 0.58% Cu, 145ppm Ag and 2.2ppm Au, is located in western Tasmania. It is hosted within a Middle Cambrian post-collisional succession of predominantly submarine, calc-alkaline volcanic and non-volcanic sedimentary rocks. The ore occurs as single or stacked, sulphide and barite-rich lenses with podiform to sheet-like morphologies, distributed over 3km of strike and >1.5km depth below the current surface.

The basal stratigraphic unit of the east-dipping mine sequence (the footwall volcanics) comprises a syn-eruptive succession of thick rhyolitic pumiceous mass flow units that were rapidly emplaced on the seafloor, and succeeded by rhyolitic to dacitic turbiditic mass flow and suspension settled volcanoclastic sediments of the transitional stratified volcanoclastics (TSV). The quartz and lithic content of the TSV increased with time as sediment provenance became more distal. The base of the Hangingwall Volcanoclastics was marked by a reduced volcanoclastic influx and deposition of a carbonaceous mudstone, followed by further volcanoclastic mass flow units with a distal clastic provenance. Intrusion of rhyolitic to dacitic peperite sills occurred prior and subsequent to the onset of mineralisation. The current study has shown that syn-depositional displacement of the sediments occurred as the result of basement faulting and sill emplacement, with cessation of significant fault movement prior to deposition of the Hangingwall Volcanoclastics. The mine sequence is truncated at the upper and lower margins by major Devonian reverse faults. Mineralisation is hosted within sediments at the top of the footwall volcanics and within the TSV.

Regional low-temperature diagenesis commenced upon deposition of the volcanoclastic sediments. Hydrothermal circulation through unconsolidated volcanoclastic sediments commenced prior to sediment compaction and lithification, locally preserving uncompacted vitriclastic textures. Hydrothermal alteration proximal to ore comprises a halo of quartz \pm sericite \pm Mn/Fe-carbonate assemblages, with a thin discontinuous chlorite assemblage located immediately beneath sulphide ore. The current study has identified a transgressive zone of intense quartz-rich alteration beneath P lens that now delineates what was a zone of fluid upflow along a syn-depositional fault. A broad halo of sericite-rich alteration envelops the ore and proximal alteration assemblages, but does not extend into the Hangingwall Volcanoclastics, as the hydrothermal system had waned prior to their emplacement.

Isotopic data indicates a hydrothermal fluid derived through the modification of seawater as it circulated through the Cambrian volcanic succession and underlying Precambrian basement, from which sulphur and metals were leached. At the mine scale, diffuse hydrothermal upflow was loosely focussed along syn-sedimentary faults defined during this study, resulting in the localisation of ore lenses along the margins of a fault-bounded basin. Significant lateral fluid flow within ~200m of the seafloor was promoted by sediment stratification, thick packages of

fine-grained sediment, peperitic sills and the development of stratiform alteration zones. Lateral movement of hydrothermal fluids was focussed along coarser, more permeable horizons within the sediments. This resulted in stratiform zones of alteration and mineralisation, and in the intense alteration of the lower margins of a peperitic quartz-feldspar-phyrlic sill and a thick siltstone package now overlying the northern ore lenses.

The current study has identified features within the northern part of the mine that indicate a sub-seafloor mode of ore formation, including: massive barite and sulphide lodes that are hosted within rapidly emplaced mass flow and turbidite units; ore lenses that locally transgress bedding; massive sulphide ore with the same immobile element signature as enclosing mass flow sediments; and a laterally extensive halo of alteration and disseminated mineralisation that extends for hundreds of metres laterally away from massive ore, for tens of metres into the footwall, and for several metres into the hanging wall. The siting of ore lenses stratigraphically below a peperitic quartz-feldspar phyrlic sill that was emplaced prior to the onset of significant hydrothermal circulation further supports a sub-seafloor mode of ore formation. The ore and the host succession do not display any textures to indicate that mineralisation occurred on the Cambrian seafloor.

Initial primary sphalerite-galena-rich mineralisation formed under relatively low-temperature (~200-250°C) and near neutral conditions, as a hot hydrothermal fluid mixed with cooler seawater and reacted with host sediments through which it passed. This mineralisation was characterised by primitive sulphide textures, including spongiform, atoll, colloform and skeletal morphologies. Utilising the laser ablation-ICP-MS analytical technique, this phase of mineralisation was found to be characterised by a low temperature trace element signature within the sulphide minerals that includes: elevated levels of Mn-Ni-As-Ag-Sb-Au-Tl-Pb and low levels of Co-Bi in pyrite; low Co:Ni and Bi:Pb ratio values in pyrite; low levels of Cu-Fe and elevated levels of Zn-Ag-Sb-Pb in sphalerite; and low levels of Sb-Ag in galena. The low temperature sulphide and barite mineralisation locally preserved an albitised volcanoclastic plagioclase component. The low temperature sphalerite-galena mineralisation was locally overprinted by and interspersed with mineralisation formed at higher temperatures, as hot hydrothermal fluids passed through permeable horizons within the ore and adjacent sediments. This phase of mineralisation produced more coarsely crystalline pyrite textures, including anhedral to euhedral grains, aggregates, and overgrowths on earlier sulphide phases. This phase of mineralisation was also characterised by a high temperature trace element signature within sulphide minerals that included: elevated levels of Bi-Sn, moderate levels of Ni-Ag-Sb-Tl-Pb-Co, and low levels of Mn-As-Au in pyrite; elevated Bi:Pb ratio values and moderate Co:Ni ratio values in pyrite; an increased Fe content in sphalerite; and galena with elevated levels of Sb-Ag. The lateral flow of high temperature (~300°C) hydrothermal fluid within the immediate footwall to sphalerite-galena ore produced discontinuous disseminated to massive pyrite-chalcopyrite mineralisation and chlorite alteration. The footwall mineralisation

was characterised by euhedral pyrite morphologies, and a high temperature sulphide mineral trace element signature comprising: elevated Co-Bi in pyrite; elevated Co:Ni and Bi:Pb ratio values in pyrite; and high levels of Fe-Mn-Cu-Sb-Bi in sphalerite.

Sphalerite-galena ore lenses are vertically and laterally zoned, with Fe-Cu enrichment at the base and proximal to interpreted zones of hydrothermal upflow, and Au-Ag-Pb-barite enrichment at the upper and lateral margins. The zonation was due to the influence of physicochemical gradients present at the time of initial ore mineral precipitation, in combination with subsequent zone refinement processes. The vertical zonation is locally inverted.

In comparison with the northern ore lenses, a cluster of sulphide ore lenses at the southern end of the mine exhibits evidence for higher temperatures of ore formation that includes: significantly elevated average Fe and Cu contents; low average Au and Ag contents; low average $\delta^{34}\text{S}$ values (<12‰); and elevated Co, Ni and Co:Ni ratio values within footwall pyrites. This suggests that the southern ore lenses were located proximal to a major site of hydrothermal upflow at Rosebery, at the intersection of two northeast and northwest trending Cambrian faults. The peripheral ore lenses, including those at the northern end of the mine, formed at lower temperatures after mixing with a greater volume of locally circulating seawater.

Devonian deformation and metamorphism produced a pervasive cleavage, brittle-ductile faulting and folding, and syn-tectonic quartz-carbonate veining containing locally remobilised sulphides variably enriched in Au±Ag. Sulphide ore exhibits deformation fabrics at the meso- and micro-scale. Late syn- to post-deformation Devonian granite intrusion produced minor faulting and veining, and metasomatic fluids that resulted in replacement of sphalerite-galena ore with massive pyrite-pyrrhotite and magnetite-biotite ± chalcopyrite assemblages. Sulphide annealing occurred syn- to post-metasomatism. The host sequence was later subjected to brittle-ductile faulting and minor dolerite intrusion.

Acknowledgements

The first person I must thank is my wife Joanna, for her love and support during the birth of this thesis. Now I can get a haircut and a real job.

Thanks to Ross Large and Stuart Bull for their excellent supervision and guidance over the last few years. Hopefully the trace element work will be of use down the track. The other academic staff at CODES and the School of Earth Sciences were also a great help when my principal supervisors were hiding in foreign locations. Particular thanks to Bruce Gemmell, Dave Cooke, Mike Solomon, Jocelyn McPhie, Ron Berry, Garry Davidson, Marc Norman, Leonid Danyushevsky, Wally Herrmann, Cathryn Gifkins and Tony Crawford. Thanks also to Simon Stephens and Peter Cornish for their very practical assistance. To Dave Steele, thanks for keeping the beast alive against all odds.

I must thank Pasmaenco for their technical and financial support, and for access to a challenging ore body. I am especially grateful to Peter Edwards and Andrew McNeill for making most things possible. To Richard Fare, Susan King, Bronwyn Turner, Charles Carnie, Cam Graves, Hans Georgi and Rob Willis, all I can say is thanks for the technical support and for welcoming me into your homes. Some even invited me twice. Thanks also to Snake, Rowie, Gun and Bill for helping me find the drill core I needed, and for regularly checking to make sure I hadn't frozen solid.

To Skakalec and the Juggernauts, namely Andrew Wurst, Darryl Clarke, Andrew Stewart, Mike Agnew and Tim Ireland, thanks for not getting me locked up in a Turkish jail. Thanks also to Alan Wilson and Glen Masterman for helping to keep me sane most of the time. A great vote of thanks to Kim Denwer for his timely assistance and for letting me occasionally win at cards.

ii Contents

1. Abstract	i
2. Acknowledgments	iv
3. Contents	v
4. Figures	x
5. Tables	xii
6. Appendices	xii
7. Frequently Used Abbreviations etc.	xiii
1. Introduction	
1.1. Location	1
1.2. Exploration History and Mining Status	1
1.3. Previous Studies and Genetic Models	2
1.4. Study Objectives	5
1.5. Methodology	6
1.6. Thesis Structure	7
2. Regional Geology	
2.1. Introduction	10
2.2. Mount Read Volcanics	12
2.2.1. The Sticht Range Beds	13
2.2.2. The Eastern quartz-phyric sequence	13
2.2.3. The Central Volcanic Complex	13
2.2.4. The Western volcano-sedimentary sequences	14
2.2.5. The Tyndall Range Group	15
2.2.6. Andesitic to basaltic volcanics	16
2.2.7. Tholeiitic mafic rocks	16
2.3. Geochronology of the Mount Read Volcanics	16
2.4. Granites, Deformation and Metamorphism	17
2.4.1. Cambrian granites and associated porphyries	18
2.4.2. The Cambrian Delamerian deformation	18
2.4.3. The Devonian Tabberabberan deformation	19
2.4.4. Metamorphism and Devonian granites	19
2.5. Immobile Element Geochemistry of the Mount Read Volcanics	20
2.6. Tectonic Setting of Western Tasmania	23
2.7. Summary	25
3. Local geology	
3.1. Introduction	26

ii Contents

3.2. Geology of the Northern Central Volcanic Complex	27
3.2.1. The Sterling Valley and Mount Black Volcanics	29
3.2.2. The White Spur Formation	30
3.2.3. Intrusives	30
3.3. Geology of the Rosebery Mine	31
3.3.1. Previous work	31
3.3.2. The footwall volcanics	33
3.3.3. Transitional stratified volcanoclastics (TSV)	42
3.3.4. The hanging wall volcanoclastics	46
3.3.5. Intrusives	50
3.4. Structure of the Rosebery Mine	55
3.4.1. Bedding (S_0) and early compaction cleavage (S_1)	55
3.4.2. Syn-depositional faulting	55
3.4.3. Devonian deformation	57
3.4.3.1. Cleavage	57
3.4.3.2. Faulting and veining	58
3.4.4. Post-Devonian deformation	61
3.4.5. The Rosebery and Mount Black Faults	62
3.5. Summary	63
4. Alteration: - Assemblages, Distribution Timing and Mineralogy	
4.1. Introduction	65
4.2. Previous Work	65
4.3. Diagenetic Alteration	66
4.3.1. Relict smectitic, zeolitic and feldspathic assemblages	66
4.3.2. Chlorite and sericite pseudofiamme	70
4.4. Mineralisation-Related Hydrothermal Alteration	70
4.4.1. Sericite dominant alteration	71
4.4.2. Quartz \pm sericite dominant alteration	71
4.4.3. Chlorite alteration	80
4.4.4. Carbonate alteration	81
4.5. Devonian Alteration	86
4.5.1. Metamorphic and deformation-related alteration	86
4.5.2. Granite-related metasomatic alteration	89
4.6. Mineral Chemistry	95
4.6.1. Carbonate	95
4.6.2. Chlorite	97
4.6.3. Sericite	100
4.7. Alteration Halo Geochemistry	102

ii Contents

4.8. Discussion	104
4.9. Summary	104
5. Mineralisation	
5.1. Introduction	107
5.2. Previous Work	107
5.3. Ore Lens Morphology and Distribution	109
5.3.1.K lens and P lens	112
5.4. Ore Mineral Zonation	113
5.5. Ore Textures and fabrics	116
5.5.1.Disseminated mineralisation	116
5.5.2.Massive sulphide ore	116
5.5.3.Lithic fragments and barite clots	119
5.5.4.Vein-style mineralisation	120
5.5.5.Other primary textures	125
5.6. Sulphide Mineralogy and Textures	125
5.6.1.Pyrite	126
5.6.2.Arsenopyrite	137
5.6.3.Sphalerite, galena and chalcopyrite	138
5.6.4.Tennantite, tetrahedrite and other sulpho-salts	141
5.6.5.Gold and electrum	141
5.6.6.Gangue mineralogy	143
5.7. Deformation-related ore remobilisation	146
5.8. Devonian Metasomatism	149
5.9. Discussion and Summary	150
6. Metal Distribution Within the Rosebery Ore	
6.1. Introduction	155
6.2. Previous Work	155
6.3. Methodology	156
6.3.1.Results	156
6.4. Discussion	163
6.4.1.Metal associations across the ore lenses	163
6.4.2.Application of the zinc ratio	165
6.4.3.The southern ore lenses	168
6.5. Summary	168

ii Contents

7. Sulphide Trace Element Chemistry	
7.1. Introduction	170
7.2. Previous Work	170
7.3. Analytical Methods	171
7.4. Comments on LA-ICP-MS Analysis	173
7.5. Results	175
7.5.1. Pyrite	176
7.5.2. Sphalerite	180
7.5.3. Tetrahedrite and tennantite	183
7.5.4. Galena	183
7.5.5. Arsenopyrite, chalcopyrite and pyrrhotite	185
7.5.6. Discussion	185
7.5.7. Co:Ni in pyrite	186
7.5.8. Bi:Pb in pyrite and sphalerite	192
7.5.9. Tl in pyrite	194
7.5.10. Au in pyrite	195
7.5.11. Ag in galena, chalcopyrite and sphalerite	196
7.5.12. Cd, Mn and Fe in sphalerite	197
7.5.13. Trends in the tennantite-tetrahedrite series	202
7.6. Summary	203
8. Isotopes	
8.1. Introduction	205
8.2. Sulphur Isotopes	205
8.2.1. Previous studies	205
8.2.2. Current study	207
8.2.2.1. Aim	207
8.2.2.2. Analytical methods	207
8.2.2.3. Results	208
8.2.3. Discussion and interpretation	209
8.2.3.1. Rosebery $h^{34}S$ signatures	209
8.2.3.2. Rosebery $h^{34}S$ – spatial trends	211
8.2.3.3. Rosebery $h^{34}S$ – sulphur isotope geothermometry	213
8.2.3.4. Regional $h^{34}S$ trends	215
8.2.4. Sulphur isotope model – discussion	218
8.2.5. Summary	222
8.3. Carbon and Oxygen Isotopes	223
8.3.1. Whole Rock Oxygen Isotopes	226

ii Contents

8.4. Strontium Isotopes	227
8.5. Lead Isotopes	227
8.6. Summary	229
9. Discussion and Synthesis	
9.1. Previous Genetic Models	232
9.2. Devonian or Cambrian?	232
9.3. At or Below the Seafloor?	237
9.4. Regional Scale Hydrothermal Circulation	242
9.5. Local Hydrothermal Circulation	243
9.6. Mineralisation	246
9.7. The Hydrothermal Fluid	249
9.8. Other Sub-Seafloor Replacement Deposits	252
9.9. Synthesis	254
References	259

iii Figures

Figure 1.1	Rosebery location plan.	1
Figure 1.2	Genetic models - Cambrian.	4
Figure 1.3	Genetic models - Devonian.	4
Figure 2.1	Bedrock geological map of the Mount Read Volcanics.	11
Figure 2.2	Time-space diagram.	12
Figure 2.3	Location of Devonian granites beneath Rosebery mine.	20
Figure 2.4	Representative geochemical fields - Suites I to V.	21
Figure 2.5	Hypothetical tectonic development of the Tasmanian section of south-eastern Australia shown as crustal cross-sections between 600 Ma and 480 Ma.	24
Figure 3.1	Stratigraphic relationships north of the Henty Fault.	27
Figure 3.2	Geology of the northern Central Volcanic Complex.	28
Figure 3.3	Historical stratigraphic nomenclature of the Rosebery mine sequence.	31
Figure 3.4	Stratigraphy of the Rosebery mine sequence.	32
Figure 3.5	Relict shards in altered footwall volcanics.	33
Figure 3.6	Immobile element geochemistry of the Rosebery mine sequence.	34
Figure 3.7	Footwall Volcanics.	35
Figure 3.8	Geological cross section 1440mN.	37
Figure 3.9	Geological cross section 1320mN.	38
Figure 3.10	Geological cross section 1200mN.	39
Figure 3.11	Geological cross section 1080mN.	40
Figure 3.12	Geological cross section 960mN.	41
Figure 3.13	Transitional Stratified Volcaniclastics.	43-44
Figure 3.14	Hangingwall Volcaniclastics.	48
Figure 3.15	Quartz-feldspar-phyric peperite within the TSV.	51-52
Figure 3.16	Quartz-feldspar porphyry.	53
Figure 3.17	Schematic of peperitic intrusive facies.	53
Figure 3.18	Schematic of peperitic sill emplacement.	53
Figure 3.19	Cambrian syn-sedimentary fault traces.	56
Figure 3.20	Devonian deformation.	59
Figure 3.21	Macro-scale folding interpretations.	61
Figure 3.22	Post-Devonian deformation.	62
Figure 4.1	Micro-scale alteration textures.	69
Figure 4.2	Alteration in the Rosebery mine sequence- Mineralisation-related.	72-74
Figure 4.3	Alteration cross section 1440mN.	75
Figure 4.4	Alteration cross section 1320mN.	76
Figure 4.5	Alteration cross section 1200mN.	77
Figure 4.6	Alteration cross section 1080mN.	78
Figure 4.7	Alteration cross section 960mN.	79
Figure 4.8	Alteration in the Rosebery mine sequence: mineralisation-related.	82-84
Figure 4.9	Alteration in the Rosebery mine sequence: deformation-related.	87
Figure 4.10	Geological cross section through F lens showing distribution of granite-related replacement zones.	90
Figure 4.11	Alteration in the Rosebery mine sequence: Devonian metasomatism.	91-93
Figure 4.12	Carbonate compositions.	96
Figure 4.13	Chlorite compositions.	98
Figure 4.14	Chlorite compositions.	99
Figure 4.15	Sericite compositions.	101
Figure 4.16	Downhole geochemical plots - 120R.	103
Figure 4.17	Alteration schematic.	105
Figure 5.1	Ore lens distribution and Cambrian fault traces.	108
Figure 5.2	Immobile element ratios - K lens ore samples	111
Figure 5.3	Cross Section of Rosebery ore zone at ~150mN	114
Figure 5.4	Copper and zinc distribution - 15 level.	114
Figure 5.5	Disseminated mineralisation.	117-118
Figure 5.6	Banded barite and sulphide ore.	118
Figure 5.7	Banding in sulphide ore.	121
Figure 5.8	Lithic material in sulphide ore.	122-123
Figure 5.9	Pre-deformation veins.	124
Figure 5.10	Bladed mineral textures.	124
Figure 5.11	Annealed sulphide textures.	126
Figure 5.12	Pyrite textures -framboids and overgrowths.	129
Figure 5.13	Framboid size distribution.	130
Figure 5.14	Pyrite textures -spongiform and atolls.	131-132

iii Figures

Figure 5.15	Pyrite textures -colloform and skeletal.	133-134
Figure 5.16	Pyrite textures -other.	135-136
Figure 5.17	Arsenopyrite, sphalerite, galena, tetrahedrite, electrum.	139-140
Figure 5.18	Albite occurrences in sulphides and barite.	144-145
Figure 5.19	Ore remobilisation.	147-148
Figure 6.1	Major elemental distribution in K lens ore.	157-159
Figure 6.2	Major elemental distribution within P lens ore: P6 and P7-P9 sub-lenses.	160-162
Figure 6.3	Interpreted temperature gradients across northern ore lenses.	164
Figure 6.4	Zn ratio value ($100Zn/(Zn+Pb)$) - variation with temperature and salinity.	165
Figure 6.5	Zn ratio values - cross section view of traverse 1.	166
Figure 6.6	Zn ratio values "cut-off" values.	167
Figure 6.7	Lower Zinc ratio cut off values for northern ore lenses.	167
Figure 7.1	K lens geochemical traverses.	171
Figure 7.2	Electron microprobe backscatter images of pyrite.	173
Figure 7.3	Time-resolved LA-ICP-MS data profile.	175
Figure 7.4	Histogram of TI values from LA-ICP-MS analysis of K lens pyrites.	175
Figure 7.5	LA-ICP-MS analysis scatter plots - pyrite.	178-179
Figure 7.6	Microprobe analysis scatter plots - sphalerite.	181
Figure 7.7	LA-ICP-MS analysis scatter plots - sphalerite.	182
Figure 7.8	Microprobe analysis scatter plots - tennantite-tetrahedrite.	184
Figure 7.9	Co vs Ni diagram for pyrite from Rosebery and Mt Lyell	187
Figure 7.10	LA-ICP-MS analysis scatter plots - Co and Ni in pyrite.	187
Figure 7.11	Southern ore lenses - 300 ppm Co in footwall pyrites.	188
Figure 7.12	Average Co vs Ni values in pyrite of sedimentary/diagenetic and submarine hydrothermal origin.	190
Figure 7.13	Average Co vs Ni values in pyrite of Devonian origin - Tasmania.	191
Figure 7.14	LA-ICP-MS analysis scatter plots - Bi and Pb in pyrite.	193
Figure 7.15	Fe vs Cu in sphalerite from various Tasmanian deposits.	198
Figure 7.16	Fe content of sphalerite vs elemental ratios and contents of pyrite.	200
Figure 7.17	Fe content of sphalerite vs Fe content of tennantite-tetrahedrite series.	200
Figure 7.18	Relationship between As-Sb and Ag-Cu in Rosebery tennantite-tetrahedrite series.	202
Figure 7.19	Fe content of sphalerite vs presence of tennantite-tetrahedrite.	202
Figure 8.1	Rosebery $d^{34}S$ data for principal stratigraphic units and ore mineralisation.	210
Figure 8.2	Average sulphide $d^{34}S$ vs metal content of major ore lenses.	212
Figure 8.3	Average sulphide $d^{34}S$ vs metal content of major ore lenses.	212
Figure 8.4	Sulphur isotope temperature estimates.	214
Figure 8.5	$d^{34}S$ data for Cambrian and Devonian deposits in western Tasmania.	216
Figure 8.6	Model of sulphur circulation in hydrothermal cell.	219
Figure 8.7	Rayleigh isotopic fractionation of Cambrian seawater.	220
Figure 8.8	Carbon and oxygen isotopes - Rosebery carbonate.	224
Figure 8.9	Carbon and oxygen isotopes - Cambrian vs Devonian systems.	224
Figure 8.10	Pb isotope data - Cambrian vs Devonian.	228
Figure 8.11	Pb isotope data - Cambrian vs Devonian.	228
Figure 9.1	Hydrothermal fluid pathways - P lens.	245
Figure 9.2	Hydrothermal fluid pathways - K lens.	245
Figure 9.3	Fluid pathways - P lens	246
Figure 9.4	fO_2 - pH diagrams for hydrothermal fluid at 250°C and 300°C.	251
Figure 9.5	Temperature vs a_{K+}/a_{H+} diagram.	251
Figure 9.6	Development of the Rosebery mine stratigraphy and ore mineralisation.	255-256

iv Tables

Table 2.1	Age data for lithostratigraphic units of the Mount Read Volcanics.	17
Table 3.1	Stratigraphy of the Hangingwall Volcaniclastics for the Bastyan Dam-Rosebery-Dalmeny area.	47
Table 4.1	Alteration types and their relative timing, Rosebery-Hercules area	67
Table 4.2	Temperatures of diagenetic mineral development	68
Table 4.3	Micro-scale alteration textures	81
Table 5.1	Electrum and gold mineral associations.	142
Table 5.2	Rosebery mineralisation paragenesis.	152
Table 7.1	Electron microprobe and LA-ICP-MS results - pyrite.	176
Table 7.2	Elemental correlation trends - pyrite.	177
Table 7.3	Electron microprobe TI analyses - pyrite.	177
Table 7.4	Electron microprobe and LA-ICP-MS analyses - sphalerite.	180
Table 7.5	Elemental correlation trends - sphalerite.	181
Table 7.6	Electron microprobe analyses - tennantite-tetrahedrite series.	183
Table 7.7	Electron microprobe analyses - galena	184
Table 7.8	Electron microprobe analyses - chalcopyrite.	185
Table 7.9	LA-ICP-MS analyses - chalcopyrite and arsenopyrite.	185
Table 7.10	Elemental ratios of Bi, Sb, Ag vs Pb - pyrite and sphalerite.	193
Table 7.11	Elemental ratios of Cd, Mn and Fe vs Zn in sphalerite - Rosebery and Devonian ores.	199
Table 8.1	Summary of sulphur isotope results from current study - K lens and P lens.	208
Table 8.2	Summary of sulphur isotope data from all units.	211
Table 8.3	Summary of sulphur isotope results from sulphide and barite lodes.	213
Table 8.4	Summary of carbon and oxygen isotope data in carbonate.	225
Table 9.1	Metal contents - Rosebery vs modern hydrothermal sulphides	249

v Appendices (volume 2)

Appendix 1.	Sample Catalogue
Appendix 2.	Whole Rock Analyses
Appendix 3.	Microprobe Analyses - Silicates
Appendix 4.	Microprobe Analyses - Sulphides
Appendix 5.	LA-ICP-MS Analyses - Sulphides
Appendix 6.	Sulphur Isotope Analyses
Appendix 7.	Geological Logs
Appendix 8.	Specific New Data Collected & Presented

vii Frequently Used Abbreviations etc.

Mineral Abbreviations

ab - albite

apy - arsenopyrite

ba- barite

sp - sphalerite

ga - galena

cpy - chalcopyrite

py - pyrite

po - pyrrhotite

tet - tennantite-tetrahedrite

el - electrum

fp - feldspar

qz - quartz

se - sericite

cl - chlorite

ru - rutile

to - tourmaline

Thin Section Abbreviations

rl - reflected light

tl - transmitted light

xp - crossed polar light

fov - field of view

Mine Grid Datum

0mE, 0mN, 0mRL = 378870.55mE, 5374181.69mN, -3049.49mRL (AMG)

0mE, 0mN, 0mRL = 0'E, 0'N, 0'RL (old grid) = 0'E, 0'N, 10,000'RL (old grid)

Rosebery N = -11°18'10" TN